Technical University of Denmark

DTU

Investigation of the maximum load alleviation potential using trailing edge flaps controlled by inflow data

Fischer, Andreas; Aagaard Madsen , Helge

DTU Library
Technical Information Center of Denmark

Investigation of the maximum load alleviation potential using trailing edge flaps controlled by inflow data

A Fischer[1], H A Madsen[1]

[1] Department for Wind Energy, Technical University of Denmark, Frederiksborgvej 399, DK-4000 Roskilde

E-mail: `asfi@dtu.dk`

Abstract. The maximum fatigue load reduction potential when using trailing edge flaps on mega-watt wind turbines was explored. For this purpose an ideal feed forward control algorithm using the relative velocity and angle of attack at the blade to control the loads was implemented. The algorithm was applied to time series from computations with the aeroelastic code HAWC2 and to measured time series. The fatigue loads could be reduced by 36% in the computations if the inflow sensor was at the same position as the blade load. The decrease of the load reduction potential when the sensor was at a distance from the blade load location was investigated. When the algorithm was applied to measured time series a load reduction of 23% was achieved which is still promising, but significantly lower than the value achieved in computations.

1. Introduction

Today most of the wind energy is produced by turbines with rotor diameters of more than 80m and a rated power of 2MW and above. And the trend goes towards increasing size. Due to the large size of the wind turbine rotor in combination with wind shear and turbulence the blades are subject to cyclic loads which cause fatigue damage and limit the life time of the wind turbine. Reducing the fatigue loads enables a bigger rotor to be mounted on the same turbine platform and thus increase the power production. It ultimately leads to a lower cost of energy.

One of the most promising concepts to alleviate fatigue loads are trailing edge flaps. There have been various studies with aeroelastic models [1], [2], [3], [4] as well as wind tunnel experiments [5]. In 2006 former Risø DTU, now DTU Wind Energy, initiated a development work to design a system applicable to modern MW wind turbines. It resulted in the design of the Controllable Rubber Trailing Edge Flap. Some of the latest results in this project are presented in [6]. There are good chances for this technology to become implemented in the wind turbine manufactures design in a short time from now.

However, the above mentioned studies showed a considerable scatter in the absolute load reduction potential. Possible reasons for the differences in load reduction potentials are the differences in flap type, size and position, sensor type and location as well as controller implementation in those studies. We were interested to clarify what is the theoretical absolute limit of the fatigue load reduction obtainable with flaps when using inflow measurements on the blade and not having any constraints on the flap. For this purpose we developed an ideal feed

forward control algorithm which can be applied to a time series of blade loads obtained from computations or measurements. When the ideal upper limit has been found it is then possible to obtain detailed information about what e.g. constraints on flap amplitude, flap angle velocity means for the load alleviation level. Furthermore, we investigated how the positioning of the inflow sensor relative to the blade load location influences the load reduction potential and the useful frequency band width of the control signal.

This paper is structured in the following way: In section 2 we describe the methods we used in our investigation. First, the aeroelastic code HAWC2 is outlined. A short overview of the measurement database used for the comparison with the computations follows. Then we derive the ideal control algorithm. This section concludes with a reminder of the fatigue load theory. Section 3 contains the results. We look into the power spectral density and the coherence function of the normal force along the blade span. This analysis helps to conclude about the ideal frequency band width of the control signal and the ideal distance between inflow sensor and blade location. In the second part of the result section we address some issues of the ideal control algorithm and the fatigue loads. Subsequently, we compute the fatigue loads along the blade of a 2MW wind turbine. We compare the results to corresponding ones of a 5MW wind turbine to detect upscaling effects and we compare the computations with measurements. In section 4 we discuss the results, point out their significance and draw conclusions.

2. Methods

2.1. HAWC2 computations

HAWC2 is an aeroelastic code for horizontal axis wind turbines [7]. The structural part is based on a multibody formulation. Arbitrary large rotation of the bodies can be handled. The bodies are assembled of Timoshenko beam elements. The aerodynamic model is based on the classic blade element momentum theory. But the theory was extended to include the effects of dynamic, skewed and sheared inflow as well as large deflections and dynamic stall of the blades. The code can simulate trailing edge flaps on the blade. For more details of the code the reader is referred to [7].

Computations were carried out for two different wind turbines, the NREL 5MW reference wind turbine [8] and the NEG-Micon NM80 wind turbine [9]. The structural model for HAWC2 of the NREL turbine was developed based on the information given in [8] and internally verified at DTU Wind Energy. The structural model for HAWC2 of the NM80 turbine is described in [10].

If the computations were compared to measurements, the inflow conditions in HAWC2 were adjusted to match the measurements of a meteorological mast on the site. The wind velocity profile in HAWC2 was given by a power law and the exponent was chosen to match the measured wind profile as close as possible. Further, the turbulence intensity was chosen to fit to the measurements with sonic anemometers. But in HAWC2 the turbulence intensity is constant with the altitude while it often varied in the measurements.

The spectral characteristics of turbulence are described by the Mann turbulence model [11] in HAWC2. The length scale L of the Mann turbulence model was set to $L = 29.4m$ and the eddy life time parameter to $\Gamma = 3.9$ according the recommendation for normal atmospheric conditions in [7]. It is possible to optimize these parameters to give the best fit to the turbulence spectra measured with the sonic anemometers, but the bad quality of the measurements in the low frequency range caused unrealistic results and the attempt was dropped.

Both wind turbines were run with constant rotational speed in the simulations. The rotational speed of the NM80 turbine was adjusted to match the rotational speed of the experiment. The rotational speed of the NREL turbine was set to the value the controller proposed in [8] enforces in steady operation.

2.2. DAN AERO measurements

The measurements presented in this paper were carried out in the DAN-AERO MW project, funded by the Danish Energy Research programme EFP-2007 under contract Journal no. 33033-0074. The project was carried out in the period from March 2007 to December 2009 in corporation between Risø DTU, now DTU Wind Energy, and the companies LM Wind Power, Vestas Wind Systems, Siemens Wind Power and DONG Energy.

We present measurements of inflow and blade section pressure on the NEG-Micon NM80 turbine. The three bladed turbine has a rotor diameter of 80m and the hub height is 57m, the nominal power is 2.75MW. The turbine was placed in a small wind farm of 8 turbines at Tjæreborg, about 1km away from the west coast of Jutland, Denmark. There was a meteorological mast in the close vicinity of the test turbine to provide detailed measurements of the wind conditions.

A new blade with identical shape as the previous blades, but equipped with measurement devices for very detailed experiments, was manufactured for the campaign. We analyzed the normal force obtained from surface pressure measurements made with pressure tabs at radial position r=13m, 19m, 30m and 37m and the local inflow vector at the blade measured with four five-hole pitot tubes at radial position r=14.5m, 20.3m, 31m and 36m, figure 1. For details of the

Figure 1. The blade of the NM80 turbine equipped with measurement devices.

experiment the reader is referred to [9].

2.3. Ideal Control Algorithm

The ideal feed forward control algorithm uses the measured relative velocity V_r and angle of attack α at a blade section to control the normal force F_N. In this theoretical study the formula is applied locally at the blade section. No assumption about the flap size is made. The relation between the normal force F_N and the inflow V_r and α is given by

$$F_N = \frac{1}{2}\rho V_r^2 C_N(\alpha)c \tag{1}$$

where C_N is the normal force coefficient and c is the chord length of the blade section. Hence, we define the controlled force as

$$F_{Nc} = F_N - f_c V_r^2. \tag{2}$$

The control parameter f_c can then be derived by a Reynolds decomposition of the variables F_N, V_r and C_N in equation 1 into mean and fluctuating part. It reads

$$f_c = K_\alpha(\alpha - \overline{\alpha}) + K_{V_r}\left(\frac{V_r^2 - \overline{V_r}^2}{V_r^2}\right). \tag{3}$$

K_α and K_{V_r} are control constants determined by numerical optimization. The numerical optimization minimizes the objective function $\langle F_{Nc}^2 \rangle$. The overline denotes the mean value which is derived in practice by band stop filtering the time signal of the quantity. A second, third or fourth order Butterworth filter transfer function was created to filter the data. After filtering the data in forward direction, the filter sequence was reversed and run back through the filter. The resulting data has zero phase distortion and the magnitude of the filter transfer function equals the squared magnitude of the Butterworth filter transfer function [12].

This way of defining a control algorithm corresponds to an unlimited local pitch actuator, meaning that the local inflow measurements are used to control the local pitch. The control strategy outlined above can also be used for a flap actuator. The relation between the control parameter f_c and the flap set angle is

$$\Delta\beta = \frac{4f_c}{\rho c \Delta C_{N,\alpha}}. \tag{4}$$

$\Delta C_{N,\alpha}$ is the change of the normal force coefficient with the angle of attack and can be estimated as 2π in the first approach.

2.4. Fatigue Load Calculation

One can define an equivalent load range R_{eq} and the corresponding number of load ranges n_{eq} which causes the same fatigue damage as the load spectrum of a given time series according to the classical theory of Palmgren-Miner and Wöhler. The equivalent load range can be used to compare the fatigue damage caused by a time series of the normal force or the blade root bending moment with and without flap control. It was derived in [13] and is given by

$$R_{eq} = \left(\frac{\sum n_i R_i^m}{n_{eq}}\right)^{1/m}. \tag{5}$$

We applied a Rainflow counting algorithm [14] to the time series to determine the set of load Ranges R_i and their number of occurrence n_i. The Wöhler exponent m describes the properties of the material exposed to fatigue damage. For example, the exponent of $m = 3$ should be applied for steel and $m = 12$ for fiber glass composites.

3. Results

3.1. Blade Loads

During operation with constant rotational speed, the power spectral density (PSD) of the normal force on the blade is peaked at multiples of the the rotation frequency, as seen in a computation for the NM80 wind turbine, figure 2. To control the normal force distribution on the blade we are also interested in the coherence function of the normal force between several positions on the blade. It gives an indication of how the spacing between sensors should be to reduce the fluctuations of the normal force. Figure 3 shows this coherence function relative to the reference position 30.37m. There is a high coherence coefficient for frequencies corresponding to multiples of the rotational period. For frequencies in between the coherence coefficient is low. This is due to the rotational sampling of the turbulence where turbulence structures bigger than the rotor
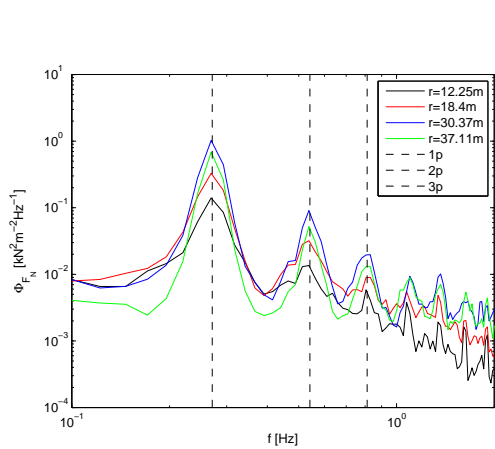
Figure 2. PSD of the normal force from computation for the NM80 wind turbine.
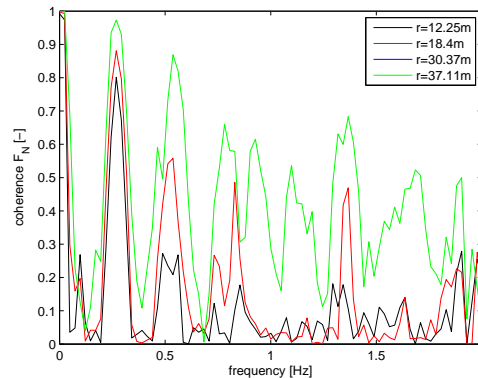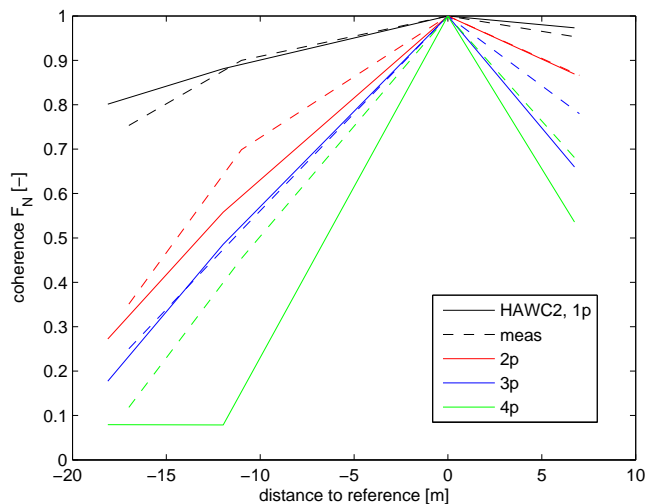

Figure 3. Coherence of the normal force relative to the reference position r=30.37m from computation for the NM80 wind turbine.

diameter will be passed several times by the rotating blade.

The coherence coefficient is smaller if the distance to the reference position is larger and the frequency range with high coherence becomes smaller. The coherence coefficient of the normal force at position r=30.37m and r=37.11m is high for frequencies corresponding up to about 5 times the rotational period (5p), while at positions r=30.37 and r=12.25 the coherence is only high for frequencies corresponding to 1p.

The peak value of the coherence coefficient for multiples of the rotation period as function of the distance to the reference position is displayed in figure 4. It is also compared to measurements to validate the HAWC2 model. The agreement between measurement and HAWC2 is excellent

Figure 4. peak value of the coherence of the normal force for multiples of the rotation period (reference position r=30.37m) for the NM80 wind turbine (measurement: dashed lines, computation: solid lines).

for frequencies up to 3p. For frequencies corresponding to 4p there is a discrepancy, but the value of the coherence coefficient is also very low. Hence, it might be due to an uncertainty in the computation of the coherence function. We have a good accuracy in simulating the unsteady loads from inflow turbulence and conclude that the modeling of unsteady aerodynamics works well in HAWC2.

The coherence coefficient for 1p frequencies is high at all blade positions. Only one inflow sensor could be sufficient to alleviate the fluctuations of the normal force for 1p. But for higher frequencies the coherence coefficient drops significantly with distance. We need more than one sensor distributed along the blade to alleviate those high frequency fluctuations.

3.2. Load Alleviation with Ideal Control

3.2.1. Control Constants The control constants were obtained by numerical optimization as described in section 2 of one ten minutes time series. We found that the control constants K_α and K_{V_r} were sensitive to the position of the inflow measurement and the position of the blade load. If we performed the numerical optimization with a time series of the inflow measurement at a fixed position and time series of the normal force at different sections of the blade, the obtained values of K_α varied by up to 200% and K_{V_r} by up to 300%. Hence, it is necessary to tune the control constants for each different position of inflow and blade load.

The control constant K_{V_r} showed also a variation about 50% when the numerical optimization was performed for time series with different wind speed at hub height, i.e 6m/s, 7.06m/s and 8m/s. K_α was invariant to changes in wind speed. A further investigation of the control equation 3 is recommended. For the present implementation of the control equations K_{V_r} has to be a function of the mean wind speed.

3.2.2. Reduction of the Fatigue Loads and Flap Activity The fatigue loads were computed for simulations of one hour time series according to the standard [15]. We computed the equivalent fatigue load amplitude of a 1Hz modulation for a given time series according to equation 5, denoted by S_1 for the original blade normal force coefficient and S_{1c} for the controlled blade normal force. The reduction of the equivalent fatigue load for the NM80 turbine operating at constant rotation and a mean wind speed at hub height of 7.06m/s is shown in figure 5. The band width of the control signal was chosen to include 1p and 2p (bw1), 1p to 3p (bw2)
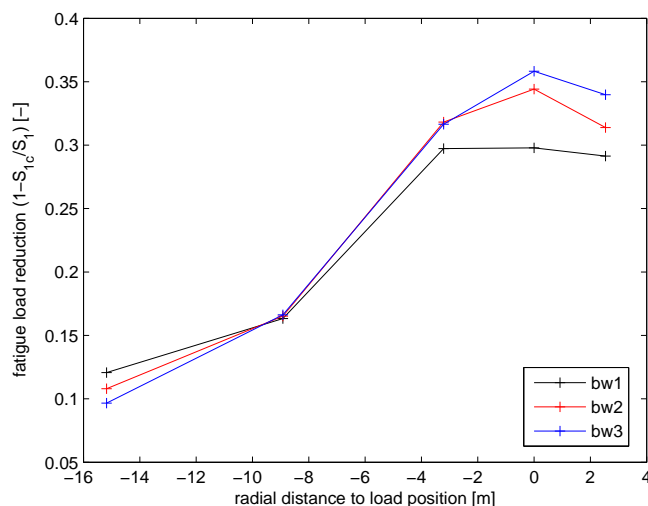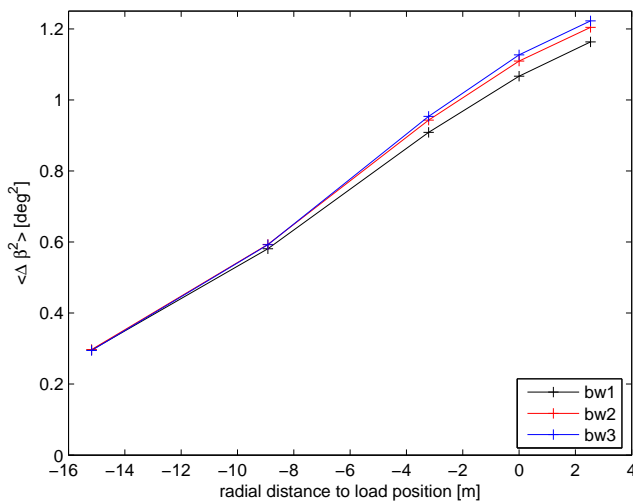

Figure 5. Reduction of the equivalent fatigue load of the blade sectional normal force (Wöhler exponent m=10) as function of the blade normal force position and bandwidth of the control signal. Inflow measured at r_i=33.58m. Legend: bw1 : 0.1-0.6Hz, bw2 : 0.1-0.9Hz, bw3 : 0.1-1.2Hz.

and 1p to 4p (bw3). Using the largest band width (bw3) we obtain the highest fatigue load reduction if the load position is close to the position of the measurement. If the load position is more than 4m away from the inflow measurement position, there is no longer any advantage in including 4p in the band width of the control signal. At this separation distance the two signals are too incoherent at the 4p frequency to allow a load reduction. Our conclusion is supported by figure 4 showing that the coherence coefficient for 4p decreases very quickly with distance.

If the inflow sensor measurement position is very far away from the blade load position, the control signal with bw1 gives the highest fatigue load reduction. The normal force and inflow signal are incoherent at high frequencies and the control introduces additional disturbance if high frequencies are included in the control signal. In this case it is beneficial to limit the band width of the control signal.

We evaluated the flap activity by computing the standard deviation of the flap set angle $\Delta\beta$. The flap activity is lower at positions close to the measurement position when the band width is reduced, figure 6. When moving further away from the measurement position it becomes
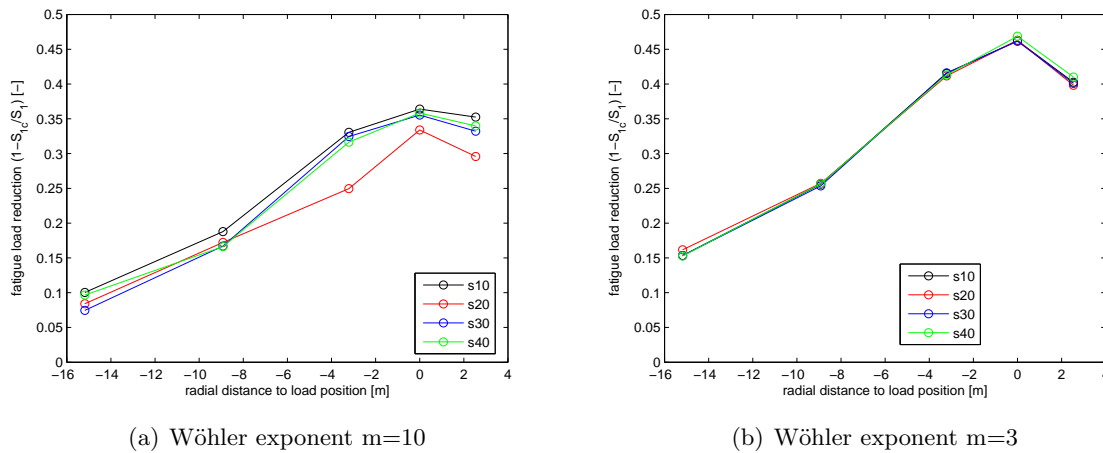

Figure 6. Flap activity as function of the blade normal force position and bandwidth of the control signal. Inflow measured at r_i=33.58m. Legend: bw1 : 0.1-0.6Hz, bw2 : 0.1-0.9Hz, bw3 : 0.1-1.2Hz.

independent of the band width. Hence, when the blade load position is close to the inflow measurement position the benefit of a higher fatigue load reduction has to be paid with a higher flap activity. When the blade load position is far away from the measurement position, a higher fatigue load reduction is achieved with equal flap activity when the band width of the control signal is limited to 2p.

*3.2.3. Non Linearity of Fatigue Loads* The behaviour of the fatigue loads depends on the Wöhler exponent m. They are highly non-linear for large values. Figure 7(a) illustrates the variation of the fatigue load reduction when we chose a realistic Wöhler exponent for wind turbine blades (m=10) and run simulation with different seeds of the turbulent time series, but keeping the statistical properties of the turbulence field. It means that the fatigue load computation is not statistically converged and a larger time series is necessary. If we choose a smaller Wöhler exponent of m=3 (figure 7(b)) the fatigue load reduction is independent of the seed used for the simulation. In this case the fatigue load calculation is statistically converged. A shorter time series is sufficient, because equation 5 is less non linear for m=3 than for m=10. Note that the fatigue load reduction is higher when m=3 is chosen than if m=10 is chosen. This result is counter intuitive. The reason is the statistical uncertainty for the fatigue load calculation with m=10.

3.2.4. Comparison of NM80 and NREL5MW Turbine We computed the fatigue load reduction for the bigger NREL 5MW wind turbine and compared the results to the ones obtained for the NM80 turbine to investigate upscaling effects. The mean wind speed at the hub height of the NM80 turbine of 7.06m/s was kept and extended according to the power law to altitudes covering the rotor of the NREL turbine. The comparison was preformed at the same absolute

(a) Wöhler exponent m=10

(b) Wöhler exponent m=3

Figure 7. Reduction of the equivalent fatigue load of the blade sectional normal force as function of the blade normal force position and turbulence seed number of the simulation. Inflow measured at r_i=33.58m. Band width of control signal 0.1-1.2Hz.
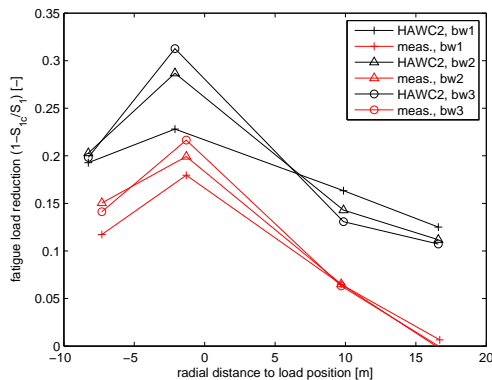
blade position, figure 8. The band width of the control signal was chosen to include frequencies
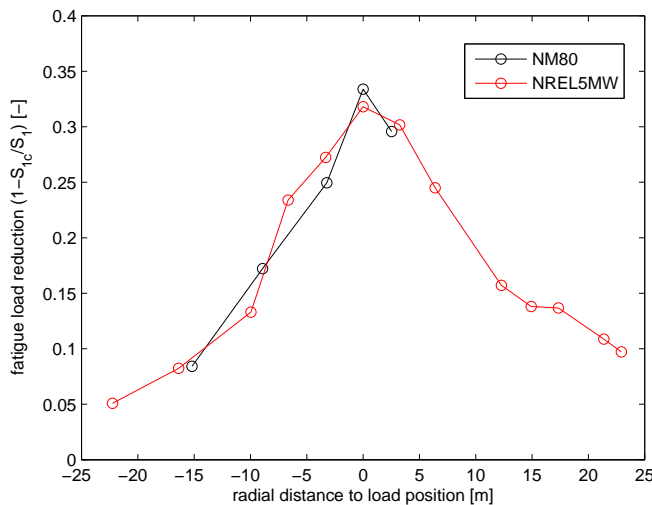
Figure 8. Reduction of the equivalent fatigue load of the balde sectional normal force (Wöhler exponent m=10) as function of the blade normal force position for the NM80 and NREL5MW turbine. Inflow measured at r_i=33.58m (NM80) and r_i=35.74m (NREL). Band width of control signal 0.1-1.2Hz (NM80) and 0.1-0.61Hz (NREL).

up to 4p for both wind turbines. The decrease of the fatigue load reduction potential when moving away from the position of the inflow sensor is almost identical for both wind turbines. The fact that the inflow sensor is placed close to the tip of the rotor of the NM80 turbine, but in the radial center of the blade of the NREL turbine has no influence on the load reduction potential. We conclude that a wind turbine with a large rotor needs more inflow sensors than a turbine with a smaller rotor.

3.2.5. Comparison of Ideal Inflow with Real Measured Inflow We applied the control algorithm on a time series of measured normal force and inflow. The inflow measurements at radial position r_i=20.3m were of the best quality. Hence we chose this position for the comparison with HAWC2 computations, figure 9. Note that the fatigue loads were obtained from 10 minute time series in
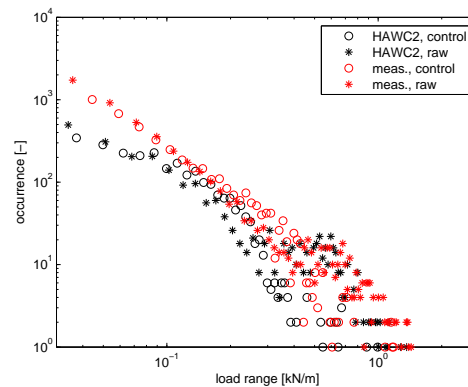
Figure 9. Reduction of the equivalent fatigue load of the blade sectional normal force (Wöhler exponent m=10) as function of the blade normal force position for the NM80 turbine from HAWC2 and measurement. Inflow measured at r_i=20.51m (HAWC2) and r_i=20.3m (meas.). Legend: bw1 : 0.1-0.6Hz, bw2 : 0.1-0.9Hz, bw3 : 0.1-1.2Hz.

Figure 10. Number of fatigue cycles (Rainflow counting) as function of the load range for the NM80 turbine from HAWC2 and measurement. Blade position r_F=18.4m (HAWC2) and r_F=19m (meas.). Inflow measured at r_i=20.51m (HAWC2) and r_i=20.3m (meas.). Band width of control signal 0.1-1.2Hz.

this comparison due to the availability of measurement data. For the measured time series the achieved fatigue load reduction is much lower than for the computed time series. The qualitative behaviour in terms of band width of the control signal and distance from the measurement position is similar. As the correlation function of the normal force from computation and measurement was in excellent agreement, we expected the computed and measured fatigue load reduction potential to be in better accordance. A closer look at the fatigue cycles is necessary. The Rainflow counting plot of load range and occurrence, figure 10, shows that the reduction of the fatigue loads is achieved by reducing the peak of the spectrum in the high load range. The reduction is more effective for the computed time series as the controlled computed spectrum rolls steeper off than the controlled measured spectrum while the spectra of the raw signals are very similar in the high load range. The number of fatigue cycles is generally higher for the measurements than for the computations, especially in the low load range. However, further investigation is needed to clarify this problem.

4. Discussion and Conclusions
An ideal feed forward control algorithm using inflow measurements on the blade was applied to determine the maximum fatigue load reduction obtainable by trailing edge flaps. We achieved a fatigue load reduction of 36% (Wöhler exponent m=10) in computations with HAWC2 of the NM80 wind turbine when the inflow was measured at the same position as the blade load. The absolute value of the fatigue load reduction was strongly dependent on the chosen Wöhler exponent. I.e. we obtained a fatigue load reduction of 47% for a Wöhler exponent of m=3. A Wöhler exponent of m=3 is not representative for the system, but the fatigue load computation with m=3 was better converged than with m=10, because of the length of the simulation time. The value for m=3 might be more representative for the possible load reduction.
The ideal band width of the control signal is a function of the separation distance of the blade load and the inflow sensor. Frequencies corresponding to four times the rotation frequency

should only be included in the control signal if the inflow sensor is less than 4m away from the blade position for the NM80 turbine. Three times the rotational frequency should only be included in the control signal if the inflow sensor is less than 8m away. The coherence of the blade normal force as function along the blade shows a steeper decrease for high frequencies than for low frequencies.

Computation of the NM80 turbine were compared to computations of the bigger NREL 5MW turbine to explore upscaling effects. The fatigue load reduction was very similar in the absolute value and followed the same function in terms of absolute distance. The relative position on the blade and the relative distance to the inflow sensor were not relevant. The main conclusion from this comparison is that bigger wind turbines need more inflow sensors than smaller ones.

HAWC2 computations of the NM80 turbine were compared to measurements. The coherence function of the blade normal force at several radial stations were in excellent agreement. The modeling of unsteady aerodynamics works well in HAWC2. However, 10% less fatigue load reduction was achieved when the algorithm was applied to a measured blade normal force and inflow time series. The qualitative behaviour of the load reduction with respect to separation to the inflow sensor was in agreement with the computation. We explored the load ranges and their occurence of the measured and computed normal force series obtained from the Rainflow counting algorithm to explain the difference in fatigue load reduction. The reduction of the number of fatigue cycles in the high load range worked better for the computed time series than for the measured time series and the overall level of the fatigue load spectrum was higher for the measured time series. We strongly recommend a more detailed analysis concerning this issue.

References

[1] Andersen P B, Hendriksen L C, Gaunaa M, Bak C and Buhl T 2008 Integrating deformable trailing edge geometry in modern mega-watt wind turbine controllers *Proc. of the EWEC2008* (Bruessels, BE)

[2] Riziotis V A and Voutsinas S G 2008 Aero-elastic modelling of the active flap concept for load control *Proc. of the EWEC2008* (Bruessels, BE)

[3] Barlas T K and van Kuik G A M 2009 Aeroelastic Modelling and Comparison of Advanced Active Flap Control Concepts for Load Reduction on the Upwind 5MW Wind turbine *Proc. of the EWEC2009* (Marseille, FR)

[4] Andersen P B 2010 *Advanced Load Alleviation for Wind Turbines using Adaptive Trailing Edge Flaps: Sensoring and Control* Ph.D. thesis Technical University of Denmark

[5] Bak C, Gaunaa M, Andersen P B, Buhl T, Hansen P and Clemmensen K 2010 *Wind Energy* **13** 207–219

[6] Barlas T K and Madsen H A 2011 Influence of Actuator Dynamics on the Load Reduction Potential of Wind Turbines with Distributed Controllable Rubber Trailing Edge Flaps (CRTEF) *Proc. of the ICAST2011* (Corfu, GR)

[7] Larsen T J and Hansen A M 2012 How to HAWC2, the users manual Tech. Rep. Risø-R-1597(ver.4-3)(EN) DTU Wind Energy, Roskilde, Denmark

[8] Jonkman J, Butterfield S, Musial W and Scott G 2009 Definition of a 5-MW Reference Wind Turbine for Offshore System Development Tech. Rep. NREL/TP-500-38060 National Renewable Energy Laboratory, Golden, Colorado, USA

[9] Madsen H A, Bak C, Paulsen U S, Gaunaa M, Fuglsang P, Romblad J, Olesen N A, Enevoldsen P, Laursen J and Jensen L 2010 The DAN-AERO MW Experiments: Final report Tech. Rep. Risø-R-1726(EN) Risø-DTU, Roskilde, Denmark

[10] Hansen M H, Fuglsang P and Thomsen K 2004 Aeroelastic modeling of the NM80 turbine with HAWC Tech. Rep. Risø-I-2017(EN)(Confidential) Risø-DTU, Roskilde, Denmark

[11] Mann J 1994 *J. of Fluid Mech.* **273** 141–168

[12] 2012 R2012a documentation matlab www.mathworks.se/help/techdoc/

[13] Thomsen K 1998 The Statistical Variation of Wind Turbine Fatigue Loads Tech. Rep. Risø-R-1063(EN) Risø National Laboratory, Roskilde, Denmark

[14] Matsuishi M and Endo T 1968 Fatigue of metals subjected to varying stress Paper presented to Japan Soc Mech Engrs, Jukvoka, Japan

[15] 2008 Wind turbines - part1: design requirements International Standard